

# Informed Circular Fields for Global Reactive Obstacle Avoidance of Robotic Manipulators<sup>\*</sup>

Marvin Becker<sup>\*</sup> Philipp Caspers<sup>\*</sup> Tom Hattendorf<sup>\*</sup>  
Torsten Lilge<sup>\*</sup> Sami Haddadin<sup>\*\*</sup> Matthias A. Müller<sup>\*</sup>

<sup>\*</sup> *Institut of Automatic Control, Leibniz University Hannover,  
Germany (e-mail: {becker,lilge,mueller}@irt.uni-hannover.de)*

<sup>\*\*</sup> *Munich School of Robotics and Machine Intelligence and Chair of  
Robotics and System Intelligence, Technical University Munich,  
Germany (e-mail: sami.haddadin@tum.de).*

**Abstract:** In this paper a global reactive motion planning framework for robotic manipulators in complex dynamic environments is presented. In particular, the circular field predictions (CFP) planner from Becker et al. (2021) is extended to ensure obstacle avoidance of the whole structure of a robotic manipulator. Towards this end, a motion planning framework is developed that leverages global information about promising avoidance directions from arbitrary configuration space motion planners, resulting in improved global trajectories while reactively avoiding dynamic obstacles and decreasing the required computational power. The resulting motion planning framework is tested in multiple simulations with complex and dynamic obstacles and demonstrates great potential compared to existing motion planning approaches.

**Keywords:** Autonomous robotic systems, Robots manipulators, Guidance navigation and control, Motion Planning, Real-Time Collision Avoidance

## 1. INTRODUCTION

*Motivation:* Classical industrial robotic applications require fences or other peripheral safety installations to ensure seamless production processes and the safety of human coworkers. However, these measures result in increasing costs and larger space requirements while decreasing flexibility. As a consequence, robots, especially collaborative systems, are increasingly exposed to dynamic and unpredictable environments requiring collision-free motion planning. However, collision avoidance of robotic manipulators in dynamic environments remains a major challenge (Liu et al., 2022).

*Related Work:* Due to the amount of research on motion planning, we focus on sampling-based and reactive approaches, using the classification of motion planners into *sense-plan-act*, *locally reactive control* and *reactive planning* (Kappler et al., 2018). Traditional approaches typically use the *sense-plan-act* paradigm with a rather strict separation of perception, motion planning and control. Most sampling-based approaches belong to this category. Among those, the rapidly-exploring random trees (RRT) algorithm (LaValle, 1998) and the probabilistic roadmap method (PRM) approach (Kavraki et al., 1996) are the most widely used concepts. The RRT algorithm incrementally constructs a search tree with randomly selected nodes in the robot's configuration space to find a feasible path from the initial to the goal pose. Due to the ease of implementation, many successful applications, and the simple extension to higher dimensional problems, the

RRT planner has been improved and extended to different variants, e.g., the RRT-connect improves the runtime (Kuffner and LaValle, 2000), whereas the asymptotically optimal RRT\* decreases the resulting path length (Karaman and Frazzoli, 2011). The PRM algorithm consists of a learning and a query phase. During the learning phase, the robot's configuration space is randomly sampled and configurations that collide with obstacles are rejected. The resulting roadmap is then used for the query phase, which calculates the shortest path from a start to a goal pose. Extensions of the PRM planner focus on improved path quality (PRM\* (Karaman and Frazzoli, 2011)) or shorter runtimes (LazyPRM\* (Hauser, 2015)). Although the improvements of sampling based planners significantly decrease computation costs and show good results even in dynamic environments, Kappler et al. (2018) has shown the advantages of reactive approaches over the classical sense-plan-act methodology, particularly in highly dynamic or uncertain environments.

While sampling-based approaches generally perform global planning, locally reactive control methods only consider obstacles in direct proximity and calculate the immediate next control command, allowing instantaneous reactions to environment changes. A widespread example is the artificial potential field (APF) approach (Khatib, 1986), where the robot is controlled by artificial repulsive and attractive forces for a collision-free motion to the goal pose. Other approaches use repulsive forces or velocities for collision avoidance of the whole structure of the robot, which were either applied on predefined control points along the robot structure (Chen and Song, 2018) or use the

<sup>\*</sup> This work was supported in part by the Region Hannover in the project *roboterfabrik*.

closest distance between robot and obstacle (Maciejewski and Klein, 1985). Another alternative is the circular field (CF) approach (Singh et al., 1996) generating artificial forces similar to forces on charged particles in electromagnetic fields. The approach gained recent interest due to its ability to smoothly guide the robot around obstacles without local minima (Haddadin et al., 2011; Ataka et al., 2018; Laha et al., 2021a,b). However, immediate reactions and local sensor information prevent locally reactive approaches from finding optimal global paths.

Kappler et al. (2018) introduce the term *reactive planner* for hybrid motion planners that are able to quickly react to local changes while simultaneously improving the global path in case of larger changes. Hybrid approaches, generally using a combination of PRM or RRT and APF, have been mainly applied in mobile robotics, e.g., (Ravankar et al., 2020), but also for manipulators (Li et al., 2021). Other hybrid approaches are the popular elastic strip framework (Brock and Khatib, 2002), or our recent circular field predictions (CFP) planner (Becker et al., 2021), which extends the CF approach with a predictive multi-agent framework for global path exploration. The CFP planner showed promising results in terms of computation load and path quality and was successfully applied on a 7-degree of freedom (DoF) manipulator. For this planner, collision avoidance and goal convergence under defined conditions were rigorously proven in Becker et al. (2022). Nevertheless, the approach was so far only used to achieve obstacle avoidance of the robot’s endeffector (EE).

*Contribution:* The contributions of this paper include:

- Extension of the CFP planner for full body obstacle avoidance of robotic manipulators by introducing additional control points along the robot structure and defining suitable control forces.
- Integration of global environment information from arbitrary global planners in the multi-agent framework from Becker et al. (2021) resulting in the informed circular fields (ICF) planner.
- Two algorithms for leveraging global information about promising avoidance directions with the reactive ICF planner.
- Extensive comparison of the ICF planner against widely used global and local motion planning approaches in a total of more than 200 simulations.

## 2. FULL BODY AVOIDANCE USING CIRCULAR FIELD PREDICTIONS

In this section, we introduce the natural extension of the CFP planner from Becker et al. (2021) for full body avoidance of a robotic manipulator. We use a steering force for controlling the EE

$$\mathbf{f}_{\text{see}} = \mathbf{f}_{\text{cf}} + k_{\text{vlc}} \mathbf{f}_{\text{vlc}}, \quad (1)$$

that consists of the CF force  $\mathbf{f}_{\text{cf}}$  (Section 2.2) for avoiding obstacles and an attractive potential force  $\mathbf{f}_{\text{vlc}}$  (Section 2.1) for goal convergence. The scaling factor  $k_{\text{vlc}} \geq 0$  of  $\mathbf{f}_{\text{vlc}}$  is explained in detail in Section 2.1. While  $\mathbf{f}_{\text{cf}}$  only contains translational forces,  $\mathbf{f}_{\text{vlc}}$  additionally includes rotational components to reach the desired goal pose.

### 2.1 Attractive Goal Force

As in Becker et al. (2021) we use the velocity limiting controller (VLC) from Khatib (1986) instead of a simple

attractive potential. This ensures that the robot moves at a constant maximum velocity during the nominal motion. Additionally, we define the scaling factor  $k_{\text{vlc}}$  as

$$k_{\text{vlc}} = \begin{cases} 0 & \text{if } \dot{\mathbf{x}} \cdot \mathbf{f}_{\text{vlc}} \leq 0 \wedge \|\dot{\mathbf{x}}\| \leq v_{\text{min}} \wedge \|\mathbf{x}_{\text{d}} - \mathbf{x}\| > \xi \\ w & \text{otherwise} \end{cases} \quad (2)$$

with the scaling factor  $w = w_1 w_2 w_3$  and  $w_1, w_2, w_3 \geq 0$  from Ataka et al. (2018), which are used to prioritize obstacle avoidance over goal convergence. The CF force does not change the magnitude of the robot velocity, which is therefore only modified by the VLC. Using Eq. (2) and therefore deactivating  $\mathbf{f}_{\text{vlc}}$  when it works against the current motion direction while the velocity is below or equal to a defined  $v_{\text{min}}$ , we ensure that the robot will only decrease its velocity below this minimum, when the robot is in the vicinity  $\xi > 0$  of the goal pose.

### 2.2 Endeffector Obstacle Avoidance

We use a similar CF force definition as Becker et al. (2021) for the obstacle avoidance of the EE and assume that obstacle data is received in point cloud format, which is commonly used by robotic sensors like depth cameras or laser scanners. The CF force for a single point on a point cloud obstacle is defined as

$$\mathbf{f}_{\text{cf}} := \frac{k_{\text{cf}}}{\|\mathbf{d}\|} \dot{\mathbf{d}} \times \mathbf{B} \quad (3)$$

with the notation  $\dot{\mathbf{d}} = \frac{\dot{\mathbf{d}}}{\|\mathbf{d}\|}$  and the constant gain  $k_{\text{cf}} \geq 0$ , the distance  $\mathbf{d} = \mathbf{x}_{\text{o}} - \mathbf{x}$  and the relative translational velocity  $\dot{\mathbf{d}}$  between the obstacle at position  $\mathbf{x}_{\text{o}}$  and the robot. The artificial magnetic field  $\mathbf{B}$  is defined as  $\mathbf{B} := \mathbf{c} \times \dot{\mathbf{d}}$  with the artificial electric current  $\mathbf{c} := \mathbf{n} \times \mathbf{b}$ , where  $\mathbf{n}$  is the normalized surface normal of the point cloud point<sup>1</sup> and  $\mathbf{b}$  is the artificial magnetic field vector, which is used to define the avoidance direction around an obstacle. The artificial magnetic field vector is therefore of crucial importance for the avoidance maneuver and different possibilities for a meaningful choice are introduced in Sections 2.5 and 3.2. The total avoidance force is the sum of the forces of all points  $m_j$  on all obstacles  $n_{\text{o}}$

$$\mathbf{f}_{\text{cf}} = \frac{1}{\sum_{j=0}^{n_{\text{o}}} m_j} \sum_{j=0}^{n_{\text{o}}} \sum_{k=0}^{m_j} \mathbf{f}_{\text{cf},j,k}. \quad (4)$$

In order to save computational resources, only obstacle points  $k$  on surfaces facing the robot, i.e.  $\mathbf{n}_k \cdot \mathbf{d}_k < 0$ , and in a range  $\|\mathbf{d}_k\| \leq d_{\text{r}}$  around the robot are used. However, in contrast to a majority of approaches in the literature, we clearly exploit more information about the obstacles than only the obstacle point with the minimum distance. This makes our algorithm less sensitive to sensor noise and yields improved avoidance behavior in the presence of multiple obstacles without oscillations.

### 2.3 Robot Body Obstacle Avoidance

To enable obstacle avoidance for the entire robot body, we define  $n_{\text{cp}}$  additional control points along its structure, as exemplarily shown for a 7-DoF robot arm in Fig. 1. The control points should be placed on prominent points of the

<sup>1</sup> Note that many approaches for the surface normal approximation of point clouds exist in the literature. We use the provided functionality of the Point Cloud Library (Rusu and Cousins, 2011).

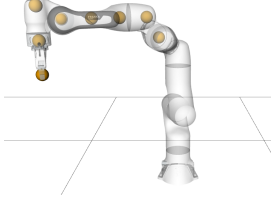


Fig. 1. Visualization of possible robot control points.

robot so that the whole structure can be moved away from obstacles. Note that for the example in Fig. 1, we have refrained from adding more control points on the lower links as their obstacle avoidance capabilities are limited. Those additional control points are also subject to the CF avoidance forces to guide them around obstacles. However, the motion of these control points may be constrained and the guiding force in Eq. (4) might not be sufficient to keep a safe distance to the obstacle. Towards this end, we add an additional repulsive CF-like force, where the artificial current is defined as the negative distance vector

$$\mathbf{f}_r := \dot{\mathbf{d}} \times (-\mathbf{d} \times \dot{\mathbf{d}}) f(\|\mathbf{d}\|), \quad (5)$$

where we use the logistic amplitude function  $f(\|\mathbf{d}\|) = \frac{1}{2}(1 + \tanh(\alpha - \beta \cdot \|\mathbf{d}\|))$  from Luo et al. (2014) with the tunable parameters  $\alpha, \beta \geq 0$ . Note that Eq. (5) is a simplification of the force from Ataka et al. (2022), which pushes the control point away from the obstacle point while maintaining the useful properties of the original CF force, i.e., it is perpendicular to the robot velocity and therefore does not induce local minima. Subsequently, the total avoidance force on a control point is  $\mathbf{f}_{cp} = \mathbf{f}_{cf} + \mathbf{f}_r$ .

#### 2.4 Robot Control Signal

In this section we describe how we generate feasible desired joint velocities for a robotic manipulator from the task space avoidance forces. Towards this end, we consider the EE motion to be the primary task and first calculate a desired joint velocity from the current EE velocity  $\dot{\mathbf{q}}_d = \mathbf{J}_{ee}^\#(\mathbf{q})\dot{\mathbf{x}}_{ee}$  using the Moore-Penrose pseudo inverse  $\mathbf{J}_{ee}^\#$ . The artificial steering force is interpreted as a force on a unit mass, i.e.,  $\ddot{\mathbf{x}}_{ee} = \mathbf{f}_{see}$ . Then, the operational space formulation from Khatib (1987) is used to calculate a meaningful robot input

$$\boldsymbol{\tau}_{ee} = \mathbf{J}_{ee}^T(\mathbf{q}) (\mathbf{M}_c(\mathbf{q})\mathbf{f}_{see} + \mathbf{c}_c(\mathbf{q}, \dot{\mathbf{q}}) + \mathbf{g}(\mathbf{q})), \quad (6)$$

with the Cartesian mass matrix  $\mathbf{M}_c(\mathbf{q})$ , the Coriolis and centrifugal terms  $\mathbf{c}_c(\mathbf{q}, \dot{\mathbf{q}})$ , and the gravitational forces  $\mathbf{g}(\mathbf{q})$ . Note that we do not consider real forces but want to transform the artificial task space forces into desired joint velocities as inputs of an appropriate joint velocity controller that compensates gravity and dynamics. Therefore, we ignore gravitational and Coriolis terms and set the mass matrix to the identity matrix  $\mathbf{I}$ , which implies  $\ddot{\mathbf{q}}_{ee} = \boldsymbol{\tau}_{ee}$  and leads to  $\mathbf{M}_c(\mathbf{q}) = (\mathbf{J}_{ee}(\mathbf{q})\mathbf{I}\mathbf{J}_{ee}^T(\mathbf{q}))^{-1}$ . Inserting  $\mathbf{M}_c(\mathbf{q})$  into Eq. (6) and neglecting the gravitation and dynamic components yields  $\ddot{\mathbf{q}}_{ee} = \mathbf{J}_{ee}^\#(\mathbf{q})\mathbf{f}_{see}$ . The forces on the control points do not need to follow any given dynamics and are superposed and converted to joint accelerations conventionally:

$$\ddot{\mathbf{q}}_{cp} = \sum_{i=0}^{n_{cp}-1} \mathbf{J}_{cp,i}^T(\mathbf{q}) \mathbf{f}_{cp,i}. \quad (7)$$

Finally, we calculate the joint velocity command for the next sampling step of the controller

$$\dot{\mathbf{q}}_{cmd} = \dot{\mathbf{q}}_d + (\ddot{\mathbf{q}}_{ee} + \ddot{\mathbf{q}}_{cp} + \ddot{\mathbf{q}}_{jla}) \Delta T, \quad (8)$$

with the sampling time  $\Delta T$ . Note that we also added a simple spring-like acceleration  $\ddot{\mathbf{q}}_{jla}$  for avoiding joint limits.

#### 2.5 Predictive Multi-Agent Framework

In order to transform the original locally reactive CF approach into a reactive planner, we extend the predictive multi-agent framework from Becker et al. (2021) to robotic manipulators. The framework is used to evaluate the influence of selected control parameters on the robot in a current perception of the environment under simplified dynamics. A predictive agent represents the robot in this environment snapshot with one specific set of parameters  $\mathbb{P}$ . In this paper we use the multi-agent framework primarily for the magnetic field vector  $\mathbf{b} \in \mathbb{B} \subset \mathbb{R}^{n_{cp} \times n_o}$  of the  $n_{cp}$  control points (including the EE). After an initial agent with the current robot configuration is created, the joint velocity commands are calculated as described in Eq. (8). Then, we simulate the motion of the robot, assuming simplified dynamics and that the controller follows the joint commands perfectly, i.e.,

$$\begin{aligned} \mathbf{q}(t+1) &= \mathbf{q}(t) + \dot{\mathbf{q}}_{cmd}(t)\Delta T \\ \dot{\mathbf{q}}(t+1) &= \dot{\mathbf{q}}_{cmd}(t) \\ \ddot{\mathbf{x}}_{ee}(t+1) &= \mathbf{J}_{ee}(\mathbf{q}(t+1))\dot{\mathbf{q}}(t+1). \end{aligned}$$

This procedure is repeated until the simulated agent reaches the goal pose  $\mathbf{x} = \mathbf{x}_d$ . Whenever the EE or a control point of the predictive agent comes close to an obstacle, i.e.,  $\|\mathbf{d}\| \leq d_r$ ,  $n_a$  new agents with different parameters are created for exploring different avoidance directions around an obstacle. All agents are evaluated after a defined number of sampling steps by a cost function, which can be adapted to the desired robot behavior and required task. The parameters of the best agent are then used to control the robot. In order to ensure reactive behavior of the planner, all agent calculations are computed in parallel to the control command of the real robot. Details on the multi-agent framework and extensive simulation results can be found in Becker et al. (2021). In contrast to our previous work, the additional control points on the robot lead to a significant increase of agents, especially in the case of many obstacles. Furthermore, many combinations of magnetic field vectors for the different control points will lead to infeasible trajectories or even to collisions. Consequently, a considerable amount of computing power is wasted. To compensate for these disadvantages, we introduce the concept of ICF in the next section.

### 3. INFORMED CIRCULAR FIELDS

The idea of ICF is to leverage the strengths of global and local motion planning strategies by extracting useful information from a global pre-planner, which are then transferred and evaluated by the predictive agents to improve the reactive motion generation. The generation of a motion command in our ICF framework can be split into four distinct phases. First, a global configuration space motion planner is used to create a (coarse) joint trajectory. Then, the global information is extracted in form of the magnetic field vectors for all control points

and obstacles as a basis for CF-based reactive motion planning. Note that when we refer to the control points here and in the following, the EE is also included if not stated otherwise. Subsequently, multiple predictive agents are created with the extracted magnetic field vectors to process and evaluate the global motion plan. The parameters of the best agent are then transferred to the real robot and used to generate the reactive joint velocity commands. The different phases are executed in parallel with different sampling rates.

### 3.1 Global Trajectory Generation

The main purpose of the global pre-planner is to infer estimates for feasible global trajectories from the current robot pose to a goal pose in configuration space, i.e., finding non-conflicting avoidance directions around the obstacles for all control points is more important than generating short and smooth paths. Thus, we use a rather coarse discretization of the global planner for shorter planning cycles  $T_{\text{global}}$ . The global planner is continuously running and restarted after  $T_{\text{global}}$  seconds with updated obstacle and robot information. When a successful trajectory is found during the planning time, the trajectory is passed to the global information extraction module. We use the MoveIt! motion planning framework for global trajectory generation because it features a variety of sampling-based planners and supports point clouds as a format for obstacle representation (Coleman et al., 2014). However, other configuration space planners can also be used and exchanged easily. Note that the global motion planning is done in a static snapshot of the environment while the actual reactive creation of the control signal (Eq. (8)) is always done with the most current environment information.

### 3.2 Global Information Extraction

Whenever the global pre-planner finds a joint trajectory, the global information extraction module transforms this joint trajectory into Cartesian trajectories for each control point. Then, the avoidance direction of each control point around each obstacle is extracted from those Cartesian trajectories and the corresponding magnetic field vectors are calculated. For each control point  $i$  and for each obstacle  $j$  described by the points  $\mathbf{x}_{o_{j,k}} \in \mathbb{O}_j \subset \mathbb{R}^{3 \times m_j}$ , the following calculations are performed.

#### Algorithm 1

- (1) Find the closest point  $\mathbf{p}_c = \mathbf{x}_{\text{cp}_i}(\tau)$  of trajectory  $\mathbf{x}_{\text{cp}_i}$  to obstacle  $j$ , where  $\tau = \arg \min_{t \geq 0} \min_{\mathbf{x}_{o_{j,k}} \in \mathbb{O}_j} \|\mathbf{x}_{\text{cp}_i}(t) - \mathbf{x}_{o_{j,k}}\|$ .
- (2) Calculate the (approximate) direction of movement  $\mathbf{v}_c = \mathbf{x}_{\text{cp}_i}(\tau + 1) - \mathbf{x}_{\text{cp}_i}(\tau - 1)$  at the closest point  $\mathbf{p}_c$ .
- (3) Calculate  $\mathbf{d}_c = \mathbf{x}_{o_{j,c}} - \mathbf{p}_c$  pointing from  $\mathbf{p}_c$  to the closest obstacle point  $\mathbf{x}_{o_{j,c}} = \arg \min_{\mathbf{x}_{o_{j,k}}} \|\mathbf{x}_{o_{j,k}} - \mathbf{p}_c\|$ .
- (4) Calculate the magnetic field vector  $\mathbf{b}_{i,j} = \frac{\mathbf{d}_c \times \mathbf{v}_c}{\|\mathbf{d}_c \times \mathbf{v}_c\|}$ .

#### Algorithm 2

- (1) Find the first point  $\mathbf{p}_{\text{in}} = \mathbf{x}_{\text{cp}_i}(\tau_{\min})$  of the trajectory  $\mathbf{x}_{\text{cp}_i}$  in a ball of radius  $r$  around obstacle  $j$ , where  $\tau_{\min} = \min_{t \geq 0, \mathbf{x}_{o_{j,k}} \in \mathbb{O}_j} (t \mid \|\mathbf{x}_{\text{cp}_i}(t) - \mathbf{x}_{o_{j,k}}\| \leq r)$ .

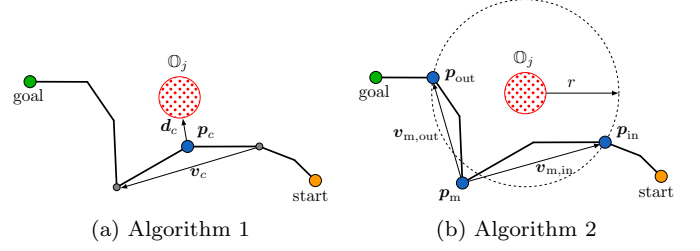


Fig. 2. Visualization of global information extraction.

- (2) Find the last point  $\mathbf{p}_{\text{out}} = \mathbf{x}_{\text{cp}_i}(\tau_{\max})$  of the trajectory  $\mathbf{x}_{\text{cp}_i}$  in a ball of radius  $r$  around obstacle  $j$ , where  $\tau_{\max} = \max_{t \geq 0} \min_{\mathbf{x}_{o_{j,k}} \in \mathbb{O}_j} (t \mid \|\mathbf{x}_{\text{cp}_i}(t) - \mathbf{x}_{o_{j,k}}\| \leq r)$ .
- (3) Find the point  $\mathbf{p}_m = \mathbf{x}_{\text{cp}_i}(\tau)$  with  $\tau$  being the largest integer less than or equal to the midpoint in  $[\tau_{\min}, \tau_{\max}]$ , i.e.,  $\tau = \lfloor 0.5(\tau_{\max} + \tau_{\min}) \rfloor$ .
- (4) Calculate the vectors  $\mathbf{v}_{m,\text{in}} = \mathbf{p}_{\text{in}} - \mathbf{p}_m$  pointing from  $\mathbf{p}_m$  to  $\mathbf{p}_{\text{in}}$  and  $\mathbf{v}_{m,\text{out}} = \mathbf{p}_{\text{out}} - \mathbf{p}_m$  from  $\mathbf{p}_m$  to  $\mathbf{p}_{\text{out}}$ .
- (5) Calculate the magnetic field vector  $\mathbf{b}_{i,j} = \frac{\mathbf{v}_{m,\text{in}} \times \mathbf{v}_{m,\text{out}}}{\|\mathbf{v}_{m,\text{in}} \times \mathbf{v}_{m,\text{out}}\|}$ .

Visualizations of both algorithms are shown in Fig. 2 in 2D example setups. The quality of the resulting avoidance motion from both methods highly depends on the environment and the global trajectory. While the first algorithm captures the avoidance motion only at the closest obstacle point, the second algorithm is used to recreate the resulting avoidance direction in a larger area around the obstacle. Therefore, we use both methods to calculate magnetic field vectors, which are adopted by the predictive agents as described in the next section. Nevertheless, we simplify a potentially complex avoidance motion to a single vector per obstacle and control point. Thus, the resulting motion of the ICF planner is expected to deviate from the global trajectory. However, we would like to emphasize again that we only use the global planner to estimate possible, non-contradictory avoidance directions, which are subsequently simulated and evaluated before being used to enable reactive control of the real robot.

### 3.3 Adapting the Multi-Agent Framework

In order to adequately account for the new information from the global pre-planner, the process for creating and deleting predictive agents (compare Section 2.5) is redesigned. Instead of creating new agents when an obstacle is encountered, new agents are created when new magnetic field vectors are received. In particular, one agent with the current best parameter set  $\mathbb{P}_{\text{best}}$  and the current best magnetic field vectors  $\mathbb{B}_{\text{best}}$  and two agents with the current best parameter set  $\mathbb{P}_{\text{best}}$  and the new magnetic field vector sets  $\mathbb{B}_{A1}$ ,  $\mathbb{B}_{A2}$  from Alg. 1 and Alg. 2 are created. Afterwards, more agents can be created to simulate the robot motion with different parameters and the three magnetic field vector sets. In this paper, new agents are created which use additional forces in the nullspace to push the robot into configurations with higher manipulability (details are omitted due to space limitations) but also simple adaptations of, e.g., the scaling factors could be simulated. Note that an agent with the best parameter set but older environment data could still exist when new agents are

created. However, the planning time of the global planner is typically much higher than the simulation of the agents and all agents finish before new magnetic field vectors are received. Moreover, the trajectory of the real robot is continuously compared to the predicted trajectories of the agents. Whenever the deviation of a trajectory point reaches a defined limit, the respective agent is deleted. Additionally, agent predictions are stopped and evaluated after a defined number of prediction steps  $n_{ps}$  and appended to the end of the waiting queue, preventing agents that take long suboptimal trajectories from blocking the available computation slots.

### 3.4 Safety-Improving Fallback

During motion planning, it may happen that none of the predicted trajectories match the current state of the environment, either because of unpredictable movements of the obstacles or because the robot cannot follow the predicted trajectories with sufficient accuracy. In this case, collision avoidance has absolute priority and the robot switches to a safety-improving fallback behavior. Here, the CF forces on the control points on the robot structure (not the EE) are replaced by repulsive forces with the scaling from Luo et al. (2014) in the form  $\mathbf{f}_{\text{crep}} = -0.5(1 + \tanh(\alpha - \beta \cdot \|\mathbf{d}\|)) \mathbf{d}$ . The safety-improving fallback is deactivated as soon as an agent finds a feasible trajectory to the goal pose.

## 4. EVALUATION

In this section, we evaluate the performance of the ICF planner in five static and dynamic environments against other reactive and global motion planning approaches. The evaluations are performed in a kinematic simulation without disturbances and with complete knowledge of the current positions and velocities of the obstacles. We use a C++ implementation on a PC with an AMD Ryzen 9 5950X CPU with 16 cores, 3.4 GHz. Our simulations include complex environments with multiple dynamic obstacles which are much easier to follow in videos than images. Thus, in addition to presenting the scenarios in Fig. 3, we uploaded videos of all simulations here: <https://doi.org/10.25835/erbbvx5h>. For the comparison, we included two different empirically chosen pre-planners within our ICF framework, the PRM and the RRT\* planner. Among the reactive control approaches, we use the original APF approach from Khatib (1986), the CF approach from Ataka et al. (2018) and our extension of the CFP from Becker et al. (2021) introduced in Section 2. Note that the safety-improving fallback and our attractive force is also implemented for the locally reactive controllers to allow a fair comparison of the force command generation. The global planners include the same sampling-based planners in their original version as used for our pre-planner, the PRM and RRT\* as well as the RRTConnect and the optimizing STOMP planner from Kalakrishnan et al. (2011) due to their high prevalence and availability in the MoveIt! framework. The sampling-based planners and the STOMP planner only consider static obstacles and are therefore only tested in the two static environments, in which a maximum planning time of 0.5s was allowed. If no solution was found in this time, the attempt was considered a failure. All non-deterministic planners were

executed until ten successful runs were recorded for each planner in each environment. Note that iteration time refers to the planning time for global planners (depicted with a \* in Table 1) while it is used to specify the calculation time for a control command for the reactive planners. Also note that the path duration depends highly on the allowed maximum velocities. While the EE velocity of the force-based methods can be specified via a Cartesian maximum velocity, the random-based planners used here operate exclusively in joint space. Specifying an EE velocity by means of constraints in the joint space is not straightforward, therefore, a measurement of the duration for the affected planners was omitted.

Overall, the results in Table 1 show that the ICF planner is able to outperform the other tested motion planners. Although its path length in static environments is (slightly) larger than the result from the optimizing STOMP planner, it still remains in a comparable range while additionally being able to reactively avoid dynamic obstacles. The advantage of the ICF planner is then particularly noticeable in the second static environment. Even though the environment does not look complicated at first, a relatively complex joint movement of the robot is required in order not to collide with the obstacles, which leads to problems of the optimizing STOMP and RRT\*, reflected in the significantly lower success rates. The CFP planner also showed problems in this environment because of the extensive number of predictive agents that were created, also noticeable in the significantly increased iteration times. Therefore, no suitable combination of avoidance directions could be found and opposing forces on the control points led to a collision. The complex environment requires simultaneous avoidance motions of the EE and the body and was meant to test the limits of the motion planners; our ICF planner was the only planner that was able to successfully reach the goal without a collision. However, as can be seen in Table 1, it was not able to succeed in all runs. The ICF planner failed when the pre-planner was repeatedly not able to find a path to the goal in the given planning time of 0.2s. Then, the ICF planner used the safety-improving fallback method and the obstacles pushed the robot into configurations which were close to the joint limits, where no avoidance was possible and a collision became inevitable. Similarly, in one execution in the environment *Dynamic 1*, the ICF-RRT\* planner ended in a configuration close to the joint limits and was not able to reach the goal afterwards.

## 5. CONCLUSION

In this paper, the CFP motion planner from Becker et al. (2021) was applied to robotic manipulators and extended to the ICF algorithm by extracting information about feasible avoidance directions from a global pre-planner. The ICF planner was tested in several simulations, where it performed well even in complex environments with multiple dynamic obstacles and demonstrated its advantage over other widespread global and locally reactive motion planners. Future research includes improving the global information extraction module, which is currently not able to extract sufficient information when more involved avoidance motions of complex obstacles are necessary. Additionally, we are working on an implementation on a real robot.



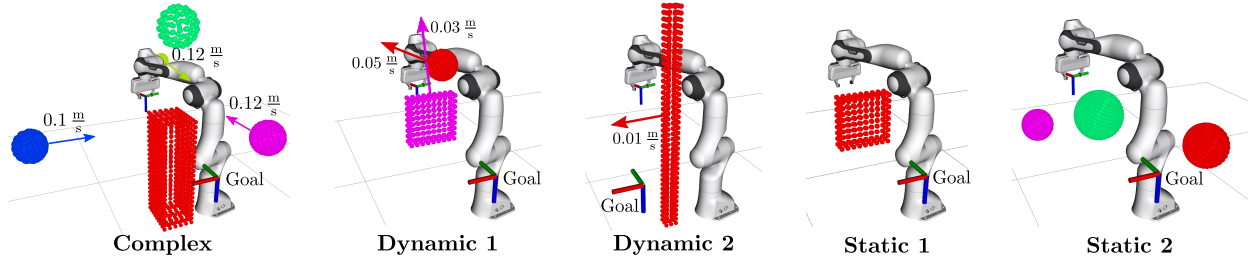


Fig. 3. Simulation environments used for comparisons.

Table 1. Motion planner comparison.

Env.	Method	Length [m]	Duration [s]	Success	Iter. Time [ms]
Static 1	PRM	1.81	-	100 %	190.0*
	RRTConnect	1.51	-	100 %	74.6*
	RRT*	1.71	-	100 %	500.0*
	STOMP	<b>1.34</b>	-	100 %	120.1*
	Khatib	1.65	17.81	True	0.020
	Ataka	1.86	19.56	True	<b>0.018</b>
	CFP	1.49	13.00	True	0.019
	ICF-PRM	1.41	11.88	100 %	<b>0.018</b>
	ICF-RRT*	1.49	<b>11.78</b>	100 %	0.019
Static 2	PRM	2.02	-	100 %	237.3*
	RRTConnect	2.01	-	100 %	257.8*
	RRT*	2.00	-	62 %	500.0*
	STOMP	<b>1.72</b>	-	43 %	163.3*
	Khatib	-	-	False	<b>0.039</b>
	Ataka	-	60.00	False	0.045
	CFP	-	-	False	0.209
	ICF-PRM	1.88	30.45	100 %	0.057
	ICF-RRT*	2.15	<b>26.51</b>	100 %	0.053
Dyn. 1	Khatib	1.50	11.46	True	<b>0.029</b>
	Ataka	1.53	10.87	True	0.030
	CFP	-	-	False	0.053
	ICF-PRM	<b>1.31</b>	<b>12.55</b>	100 %	0.035
	ICF-RRT*	1.48	13.13	91 %	0.033
Dyn. 2	Khatib	1.68	33.81	True	0.020
	Ataka	-	60.00	False	0.021
	CFP	<b>1.47</b>	12.75	True	0.029
	ICF-PRM	1.51	<b>11.96</b>	100 %	0.016
	ICF-RRT*	1.54	12.55	100 %	<b>0.014</b>
Complex	Khatib	-	-	False	0.082
	Ataka	-	-	False	0.080
	CFP	-	-	False	0.126
	ICF-PRM	<b>2.12</b>	<b>27.42</b>	<b>71 %</b>	<b>0.048</b>
	ICF-RRT*	2.20	28.46	<b>62 %</b>	0.058

## REFERENCES

Ataka, A., Lam, H.K., and Althoefer, K. (2018). Reactive magnetic-field-inspired navigation for non-holonomic mobile robots in unknown environments. In *Proc. IEEE Int. Conf. Robot. Autom.*, 6983–6988.

Ataka, A., Lam, H.K., and Althoefer, K. (2022). Magnetic-field-inspired navigation for robots in complex and unknown environments. *Frontiers in Robotics and AI*, 9.

Becker, M., Köhler, J., Haddadin, S., and Müller, M.A. (2022). Motion Planning using Reactive Circular Fields: A 2D Analysis of Collision Avoidance and Goal Convergence. *arXiv preprint arXiv:2210.16106*. doi:10.48550/ARXIV.2210.16106.

Becker, M., Lilge, T., Müller, M.A., and Haddadin, S. (2021). Circular fields and predictive multi-agents for online global trajectory planning. *IEEE Robot. Autom. Lett.*, 6(2), 2618–2625.

Brock, O. and Khatib, O. (2002). Elastic Strips: A Framework for Motion Generation in Human Environments. *Int. J. Robot. Res.*, 21(12), 1031–1052.

Chen, J.H. and Song, K.T. (2018). Collision-free motion planning for human-robot collaborative safety under cartesian constraint. In *Proc. IEEE Int. Conf. Robot. Autom.*, 4348–4354.

Coleman, D., Sucan, I., Chitta, S., and Correll, N. (2014). Reducing the Barrier to Entry of Complex Robotic Software: a MoveIt! Case Study. *J. Soft. Eng. Robot.*

Haddadin, S., Belder, R., and Albu-Schäffer, A. (2011). Dynamic motion planning for robots in partially unknown environments. *IFAC Proc. Vol.*, 44(1), 6842–6850.

Hauser, K. (2015). Lazy collision checking in asymptotically-optimal motion planning. In *Proc. IEEE Int. Conf. Robot. Autom.*

Kalakrishnan, M., Chitta, S., Theodorou, E., Pastor, P., and Schaal, S. (2011). STOMP: Stochastic trajectory optimization for motion planning. In *Proc. IEEE Int. Conf. Robot. Autom.*, 4569–4574.

Kappler, D., Meier, F., Issac, J., Mainprice, J., Cifuentes, C.G., Wüthrich, M., Berenz, V., Schaal, S., Ratliff, N., and Bohg, J. (2018). Real-Time Perception Meets Reactive Motion Generation. *IEEE Robot. Autom. Lett.*, 3(3), 1864–1871.

Karaman, S. and Frazzoli, E. (2011). Sampling-based algorithms for optimal motion planning. *Int. J. Robot. Res.*, 30(7), 846–894.

Kavraki, L.E., Svestka, P., Latombe, J.C., and Overmars, M.H. (1996). Probabilistic roadmaps for path planning in high-dimensional configuration spaces. *IEEE Trans. Robot. Autom.*, 12(4), 566–580.

Khatib, O. (1987). A unified approach for motion and force control of robot manipulators: The operational space formulation. *IEEE J. Robot. Autom.*, 3(1), 43–53.

Khatib, O. (1986). Real-time obstacle avoidance for manipulators and mobile robots. *Int. J. Robot. Res.*, 5(1), 90–98.

Kuffner, J.J. and LaValle, S.M. (2000). RRT-connect: An efficient approach to single-query path planning. In *Proc. IEEE Int. Conf. Robot. Autom.*, volume 2, 995–1001.

Laha, R., Figueredo, L.F., Vrabel, J., Swikir, A., and Haddadin, S. (2021a). Reactive cooperative manipulation based on set primitives and circular fields. In *Proc. IEEE Int. Conf. Robot. Autom.*, 6577–6584.

Laha, R., Vorndamme, J., Figueredo, L.F., Qu, Z., Swikir, A., Jähne, C., and Haddadin, S. (2021b). Coordinated motion generation and object placement: A reactive planning and landing approach. In *Proc. IEEE/RSJ Int. Conf. Intell. Robots Syst.*, 9401–9407.

LaValle, S.M. (1998). Rapidly-exploring random trees: A new tool for path planning: Technical Report.

Li, S., Han, K., Li, X., Zhang, S., Xiong, Y., and Xie, Z. (2021). Hybrid Trajectory Replanning-Based Dynamic Obstacle Avoidance for Physical Human-Robot Interaction. *J. Intell. & Robot. Syst.*, 103(3), 41.

Liu, H., Qu, D., Xu, F., Du, Z., Jia, K., Song, J., and Liu, M. (2022). Real-time and efficient collision avoidance planning approach for safe human-robot interaction. *J. Intell. & Robot. Syst.*, 105(4).

Luo, R.C., Ko, M.C., Chung, Y.T., and Chatila, R. (2014). Repulsive reaction vector generator for whole-arm collision avoidance of 7-DoF redundant robot manipulator. In *Proc. IEEE/ASME Int. Conf. on Adv. Intell. Mechat.*, 1036–1041.

Maciejewski, A.A. and Klein, C.A. (1985). Obstacle Avoidance for Kinematically Redundant Manipulators in Dynamically Varying Environments. *Int. J. Robot. Res.*, 4(3), 109–117.

Ravankar, A.A., Ravankar, A., Emaru, T., and Kobayashi, Y. (2020). HPPRM: Hybrid Potential Based Probabilistic Roadmap Algorithm for Improved Dynamic Path Planning of Mobile Robots. *IEEE Access*, 8, 221743–221766.

Rusu, R.B. and Cousins, S. (2011). 3D is here: Point Cloud Library (PCL). In *Proc. IEEE Int. Conf. Robot. Autom.*

Singh, L., Stephanou, H., and Wen, J. (1996). Real-time robot motion control with circulatory fields. In *Proc. IEEE Int. Conf. Robot. Autom.*, volume 3, 2737–2742.